6846 *Biochemistry* **2010,** *49,* 6846–6855
DOI: 10.1021/bi100598f

BIOCHEMISTRY
including biophysical chemistry & molecular biology
Article

A Solution Model of the Complex Formed by Adrenodoxin and Adrenodoxin Reductase Determined by Paramagnetic NMR Spectroscopy[†]

Peter H. J. Keizers,[‡,∥] Berna Mersinli,[§,∥] Wolfgang Reinle,[§] Julia Donauer,[§] Yoshitaka Hiruma,[‡] Frank Hannemann,[§] Mark Overhand,[‡] Rita Bernhardt,*[,§] and Marcellus Ubbink*[,‡]

[‡]*Leiden Institute of Chemistry, Gorlaeus Laboratories, Leiden University, P.O. Box 9502, 2300 RA Leiden, The Netherlands, and* [§]*Universität des Saarlandes, FR 8.8 Biochemie, Campus B2.2, 66041 Saarbrücken, Germany.* [∥]*These authors contributed equally to this work.*

Received April 19, 2010; Revised Manuscript Received July 13, 2010

ABSTRACT: Lanthanide tags offer the opportunity to retrieve long-range distance information from NMR experiments that can be used to guide protein docking. To determine whether sufficient restraints can be retrieved for proteins with low solubility and availability, Ln tags were applied in the study of the 65 kDa membrane-associated protein complex formed by the electron carrier adrenodoxin and its electron donor, adrenodoxin reductase. The reductase is only monomeric at low concentration, and the paramagnetic iron−sulfur cluster of adrenodoxin broadens many of the resonances of nuclei in the interface. Guided by the paramagnetic restraints obtained using two Ln-tag attachment sites, protein docking yields a cluster of solutions with an rmsd of 3.2 Å. The mean structure is close to the crystal structure of the cross-linked complex, with an rmsd of 4.0 Å. It is concluded that with the application of Ln tags paramagnetic NMR restraints for structure determination can be retrieved even for difficult, low-concentration protein complexes.

A basic understanding of how macromolecules such as proteins bind other macromolecules is a cornerstone in structural and systems biology. NMR spectroscopy has been used to determine the structure of small complexes, and only recently, much larger complexes have been studied. Nevertheless, improvement of the methods remains necessary, especially for the cases of challenging proteins, such as membrane-associated proteins (*1*−*4*). Other proteins that can be troublesome in NMR experiments are those containing metal cofactors. The nuclei surrounding the endogenous paramagnetic metal are usually invisible in NMR spectroscopy due to enhanced nuclear relaxation. Substitution of the metal for a diamagnetic analogue can resolve this problem (*5*), but this procedure is often accompanied with large loss of protein (*6*). In electron transfer proteins generally the metal binding site is close to the interface with the partner proteins to facilitate the electron transfer. Therefore, the interaction sites in electron transfer proteins are often difficult to study by conventional NMR. Interestingly, paramagnetism offers at the same time excellent opportunities to obtain long-range distance information (*5*, *7*). With an artificial paramagnetic Ln probe it is possible to retrieve distance restraints from far beyond the interaction site, avoiding the problem of the broadened resonances in the interface. Another important advantage of the application of a Ln tag is that the most useful paramagnetic effects, the pseudocontact shift, and the paramagnetic relaxation enhancement can be readily obtained from sensitive heteronuclear correlation experiments requiring only a low protein concentration. A prerequisite for reliable restraints is to have a rigid paramagnetic tag.

In this study, the complex of adrenodoxin reductase (AdR)[1] and adrenodoxin (Adx) is investigated. These proteins are components of the steroid hormone biosynthesis redox chain in the adrenal mitochondria of vertebrates, containing also the CYP11 family of cytochrome P450 enzymes. CYP11A1 (P450scc) converts cholesterol to pregnenolone, which is the initial and rate-limiting step of steroid hormones biosynthesis (*8*). Enzymes of the CYP11B subfamily are responsible for the formation of cortisol (CYP11B1) as well as aldosterone (CYP11B2) (*9*, *10*). These cytochromes require two electrons to catalyze oxygen cleavage and substrate hydroxylation, which are obtained from NADPH and delivered via AdR and Adx. AdR is localized at the matrix side of the inner mitochondrial membrane and membrane-bound by ionic interactions (*9*, *11*, *12*). It is a 51 kDa, NADPH-dependent, electron donor carrying FAD as a prosthetic group (*13*). The ferredoxin Adx is a 14 kDa soluble protein, consisting of 128 amino acids. Via its Fe_2S_2 cluster, Adx carries electrons from AdR to several cytochrome P450 enzymes (*10*). The crystal structure has been determined of the 4−108 truncated Adx as well as the full-length protein, which demonstrated the presence of a flexible C-terminus (*14*, *15*). The crystal structure of NADPH-bound AdR was also solved, followed by the structure of a 1:1 cross-linked complex of AdR and full-length Adx (*16*, *17*).

Here, we use the AdR−Adx complex as a test case to determine whether Ln tags can provide sufficient restraints to establish

[†]This research has been funded by the Volkswagenstiftung, Grant I/80 854, The Netherlands Organisation for Scientific Research (NWO), VENI Grant 700.58.405 (P.H.J.K.) and VICI Grant 700.58.441 (M.U.), and the Access to Research Infrastructures activity in the sixth Framework Programme of the EC (Contract RII3-026145, EU-NMR).

*To whom correspondence should be addressed. R.B.: telephone, 0049 6813023005; fax, 0049 6813024739; e-mail, ritabern@mx.uni-saarland.de. M.U.: telephone, 0031 715274628; fax, 0031 715275856; e-mail, m.ubbink@chem.leidenuniv.nl

[1]Abbreviations: Adx, adrenodoxin; AdR, adrenodoxin reductase; CLaNP-5, caged lanthanide NMR probe 5; 7-DHC, 7-dehydrocholesterol; 7-DHP, 7-dehydropregnenolone; drms, distance root mean square; rmsd, root-mean-square deviation; R_2^{para}, paramagnetically enhanced transverse nuclear relaxation rate.

 Published on Web 07/13/2010

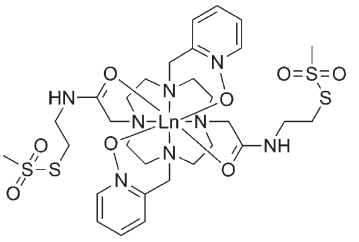

FIGURE 1: Structure of the Ln tag: caged lanthanide NMR probe 5 (CLaNP-5). The tag has been chelated to the Ln ions Eu^{3+}, Gd^{3+}, Lu^{3+}, and Tm^{3+}.

the orientation of proteins in a complex in the case of membrane-associated proteins with poor availability and including a Fe_2S_2 cluster in the interface. We demonstrate that with two Ln-tag positions sufficient information is obtained to yield a reliable model of the complex. This is the first structural model of the AdR−Adx complex in solution.

MATERIALS AND METHODS

Chemicals. Caged lanthanide NMR probe 5 (CLaNP-5) was synthesized and chelated to various Ln ions (Ln-CLaNP-5, Figure 1) as described (*18*). Superdex 75, Superdex 200, and Source 30Q columns were from GE Healthcare (Munich, Germany). All other chemicals were reagent grade commercial products and were used without further purification.

Mutagenesis and Expression of AdR Mutants. AdR mutants A, C364S/S425C/K429C, B, C364S/C145S/Q232C/K236C, C, C364S/M352C/V357C, and D, C364S/K395C/H398C were produced in cloning vector pMOSBlue, using the QuikChange site-directed mutagenesis kit (Stratagene, La Jolla, CA) and subcloned into pBar1607, using the *Nde*I/*Hind*III sites (*19*). Amplification of AdR cDNA in pMOSBlue was performed using forward and reverse primers designed according to the manufacturers' guidelines. All mutations were verified by DNA sequencing.

Protein Production. The genes for the AdR variants were heterologously coexpressed in *Escherichia coli* C43DE3 harboring pBAR1607, using the chaperone-containing plasmid pGro12 (*19*−*21*). Purification was performed as described, and protein concentration was determined using $\varepsilon_{450} = 11.3\ mM^{-1}\ cm^{-1}$ (*19*, *22*). UV/vis spectra were recorded at room temperature on a Shimadzu double-beam spectrophotometer UV2101PC using a 50 mM potassium phosphate buffer, pH 7.4, containing 0.1 mM dithioerythritol, 0.1 mM EDTA, and 0.7 M KCl. Protein fractions with an A_{270}/A_{450} ratio between 7.6 and 8.0 were collected, yielding 4 mg/L culture of wild type and 1.5−2 mg/L culture of the mutants. CD spectra of the AdR forms were obtained on a Jasco 715 spectropolarimeter at room temperature. Reaction mixtures contained 20 μM AdR in HEPES buffer, pH 7.4, containing 0.05% Tween 20. $^2H^{15}N$-enriched wild type and (4−108) truncated Adx were produced using *E. coli* BL21 and the pKKHC plasmid (*23*). The cells were grown in M9 minimal medium containing $^{15}NH_4Cl$ and either glycerol-d_3 for Adx wild type or acetate-d_3 for Adx (4−108). The D_2O content was gradually increased up to 99%. Purification was performed as described using Source-30Q anion-exchange and Superdex G75 gel filtration (*24*). Non-isotope-enriched Adx was produced as described (*25*). Adx was quantified using $\varepsilon_{415} = 9.8\ mM^{-1}\ cm^{-1}$, and protein with an A_{414}/A_{276} ratio > 0.9 was isolated (*26*). Yields were 1.4 mg/L for wild type and 2−3 mg/L for Adx (4−108). CYP11A1 was produced as described; the protein concentration was determined by carbon monoxide difference spectroscopy using $\varepsilon_{450-490} = 91\ mM^{-1}\ cm^{-1}$ (*27*, *28*).

Ln-CLaNP-5 Attachment to AdR. A solution of 0.2 mM AdR in 20 mM degassed sodium phosphate buffer, pH 7.4, containing 0.1 M NaCl, was first treated with 5 mM freshly prepared dithiothreitol for 1 h on ice. Superdex 200 gel filtration was used to remove the surplus of dithiothreitol. The resulting AdR solution was mixed with 3 mol equiv of Ln-CLaNP-5 and incubated for 1 h on ice. Surplus of Ln-CLaNP-5 and protein dimer was separated using Superdex 200 gel filtration. Protein concentration was determined by UV/vis spectroscopy. The yield after the entire labeling procedure, including purification, was about 20−25%. AdR has been labeled with Eu-CLaNP-5, Gd-CLaNP-5, Tm-CLaNP-5, and Lu-CLaNP-5 for fluorescence, paramagnetic relaxation enhancement, pseudocontact shift, and diamagnetic control measurements, respectively.

Adx Reduction. Reduction of full-length Adx was determined by UV/vis spectroscopy. Samples contained 50 μM full-length Adx, 5 μM AdR, and 50 μM NADPH. Quantitative Adx reduction was determined indirectly by measuring subsequent reduction of cytochrome *c* by Adx. The reduction of Adx by AdR is rate limiting in this experiment (*23*, *29*). Reaction mixtures contained 1 μM full-length Adx or Adx (4−108), 200 μM cytochrome *c*, and 0.05 − 1.0 μM AdR. The reaction was initiated by adding 200 μM NADPH. Cytochrome *c* reduction was monitored at 550 nm, using $\varepsilon_{550} = 20\ mM^{-1}\ cm^{-1}$ (*30*). All samples contained 50 mM potassium phosphate buffer, pH 7.4. The assays were performed on a Shimadzu double-beam spectrophotometer UV2101PC at room temperature.

Substrate Conversion. The conversion of 7-DHC to 7-DHP was performed using a reconstituted assay system (*31*), containing 1 μM AdR, 1 μM Adx, 1 μM CYP11A1, and 200 μM 7-DHC in 50 mM HEPES−Tween 20 buffer. An NADPH-regenerating system (5 μM glucose 6-phosphate, 1 U glucose-6-phosphate dehydrogenase, and 1 μM $MgCl_2$) was added, and the reaction was initiated by adding 100 μM NADPH. After 10 min incubation at 37 °C the reaction was stopped by adding one sample volume of chloroform. The steroids were extracted twice with chloroform, dried, and resuspended in acetonitrile. Aliquots were analyzed by HPLC, using a Nucleodur 100-3 C18 RP column (Macherey-Nagel) with an isocratic mixture of acetonotrile−2-propanol (30:1) and cholecalciferol as internal standard. Peak areas of product and standard at 280 nm were determined using the JASCO Borwin software.

Protein NMR. Typically, NMR samples comprised 250−300 μL in a Shigemi tube, containing 20−50 μM $^{15}N^2H$ Adx with 1.2 equiv of Ln-CLaNP-5-attached AdR in 20 mM sodium phosphate, pH 7.4, 6% D_2O (v/v), and 100 mM NaCl. [^{15}N,^1H]-TROSY spectra (*32*) were recorded at 285 K on a Bruker Avance DMX 600 spectrometer equipped with a TCI-Z-GRAD cryoprobe. Data were processed in Azara (www.bio.cam.ac.uk/azara) and analyzed in Ansig for Windows (*33*). The assignments of the resonances were based on previous work (*34*). Chemical shift perturbations ($\Delta\delta_{avg}$) were defined as described by Grzesiek et al. (*35*). The agreement between observed and back-calculated NMR parameters is expressed in a quality factor Q (eq 1), defined as the ratio of the rmsd between observed and calculated data and the rms of the sum of the observed and the calculated data (*36*).

$$Q = \sqrt{\frac{\sum_i \{\Delta\delta_{PC}^{obs}(i) - \Delta\delta_{PC}^{sim}(i)\}^2}{\sum_i \{\Delta\delta_{PC}^{obs}(i) + \Delta\delta_{PC}^{sim}(i)\}^2}} \quad (1)$$

Paramagnetic NMR. Pseudocontact shifts and paramagnetic relaxation enhancements were determined as described before (*18*). For the paramagnetic relaxation enhancements, the paramagnetic over diamagnetic intensity ratios were normalized using the resonances for residue T21, a residue with no significant broadening, surrounded by other residues with no significant broadening and located at the other side of the protein relative to the residues for which the strongest effects were observed. From the R_2^{para}, the Gd ion-to-amide proton distances were calculated using the simplified Solomon and Bloembergen equation (*37*). For 24 amides the resonances were assigned and sufficiently resolved to yield reliable paramagnetic relaxation enhancements. The obtained paramagnetic relaxation enhancements were divided in two classes of restraints. The first class (13 restraints) was formed by the amide resonances with an intensity ratio up to 0.83. For these residues the distances as determined from the paramagnetic relaxation enhancement were used (±4 Å). The second class (11 restraints) consisted of the amide resonances with an intensity ratio of more than 0.83. These residues where considered to be too far from Gd for accurate distance determination and to these were assigned a lower distance limit of 44 (−4, +100) Å. As AdR is a membrane-associated protein, it could only be concentrated to limited extent. At concentrations higher than 50 μM, significant aggregation occurred, even in presence of Adx. For this reason, for the paramagnetic relaxation enhancement analysis, the method according to Battiste and Wagner was used instead of the one of Iwahara et al. (*38*, *39*). The latter method has been reported to be less prone to artifacts, but it is less sensitive. Moreover, in our hands the one-point method yields reliable distances and has successfully been employed to determine structures of protein complexes before (*18*, *40*).

Protein Docking. To determine the solution model of the complex formed by Adx and AdR, the proteins were docked using the software XPLOR-NIH (*41*). The structure of AdR was taken from the crystal structure of the cross-linked complex (PDB entry 1E6E) and that of Adx from the crystal structure of the free protein (PDB entry 1AYF). For inclusion of the pseudocontact shift restraints, the PARArestraints module was employed, and the Prodrug server was used to create FAD parameter and topology files (*42*, *43*). Chemical shift perturbations were treated as NOE-type distance restraints. Only the Adx residues having an accessible surface area (ASA) of more than 40% were taken into account, as determined with the software NACCESS 2.1.1 (*44*). A total of 16 amides with a $\Delta\delta_{avg}$ of > 0.03 ppm were given a distance of 11 (−8/+15) Å to any amide nitrogen atom of AdR, applying the sixth power distance averaging option. The Ln-CLaNP-5 molecules and their accompanying χ-tensors were represented by a Ln ion and an axis system, made out of three pseudoatoms, representing the χ-tensor direction. The Ln ions were placed at 8 Å from the introduced Cys Cα atoms in the direction of the side chains, with the *z*-axis of the χ-tensor initially pointing away from the backbone, as described before (*18*). The magnitude of the χ-tensor of Tm-CLaNP-5 was obtained previously and amounts 55.3 and 6.9 × 10^{-32} m^3 for the axial and rhombic components, respectively (*18*). The script of the docking procedure is supplied in the Supporting Information. In short, the protein complex formed by AdR and Adx was energy minimized guided by the energy terms for the chemical shift perturbations, paramagnetic relaxation enhancements, and pseudocontact shifts. Adx started at a random position 60 ± 10 Å away from AdR, with a random rotation of 15°. The energy minimization started with a rotation of the χ-tensors, using only the pseudocontact shift energy term and keeping proteins and Ln ions fixed. Subsequently, the proteins were allowed to translate and rotate, guided by all the restraints, with the Ln ions and their χ-tensors fixed relative to AdR. The proteins were kept rigid, and only the backbone and Cβ and Cγ atoms were considered in the repel function used to avoid steric clashes. A total of 400 0.04 ps steps of restricted MD was performed at 300 K, and subsequently the χ-tensor orientations were optimized once more based on the pseudocontact shift restraints, with proteins and Ln ions fixed. This iterative minimization cycle was repeated 50000 times in a typical run. When during the minimization the total energy did not decrease for six cycles, Adx was placed at a random position 60 ± 10 Å away from AdR, with a random rotation of 15°, and minimization was continued. Structures of complexes were saved and pseudocontact shifts and paramagnetic relaxation enhancements back-calculated, when the total energy was below an energy cutoff. Only the lowest energy structure was saved per approach from a given starting position. The force constants used to scale the chemical shift perturbations was set to 50, the force for pseudocontact shifts was set to 250, and for paramagnetic relaxation enhancements it was set to 100. These were varied to yield similar energy contributions, and it was verified that both the paramagnetic relaxation enhancement and pseudocontact shift energy terms played a role in ranking the top lowest energy structures. Protein structures are visualized using Pymol (De Lano Scientific, Palo Alto, CA).

RESULTS AND DISCUSSION

Mapping the AdR Binding Site of Adx. AdR wild type was titrated into a solution of truncated $^2H^{15}N$-enriched Adx (4−108) from 0.3 to 1.2 mol equiv. After each addition, the TROSY NMR spectrum was recorded (Figure S1 of the Supporting Information). The disappearance and reappearance of shifted cross-peaks are indicative of binding in the slow exchange regime, in line with the results found before in surface plasmon resonance measurements, in which a dissociation rate constant of 0.0038 s^{-1} was determined (*25*). Due to the presence of the Fe_2S_2 cluster in Adx many resonances are broadened beyond detection. Nevertheless, several shifted cross-peaks could be assigned by comparison (*6*), and chemical shift perturbations ($\Delta\delta_{avg}$) were determined (Figure 2). Large shifts ($\Delta\delta_{avg}$ > 0.15) were observed for residues 31, 40, 42, 43, 59, 60, 72, 76, 79, 85, and 96. From the binding map, it is clear that Adx binds with its cofactor binding site toward AdR, as inferred from the surrounding ring of large chemical shift perturbations. This binding orientation is similar to the one observed in the crystal structure of the complex and in line with the role of Adx as an electron transfer protein (*14*). The stoichiometry of binding cannot be revealed from a single set of chemical shift perturbations from a protein complex in slow exchange, but the binding map is consistent with a well-defined binding site in a 1:1 complex.

TROSY spectra were also acquired of the full-length $^2H^{15}N$-enriched Adx in the absence and presence of AdR. The spectral changes observed resembled those for the truncated Adx, indicating a similar interaction (Figure S2 of the Supporting Information). Large shifts ($\Delta\delta_{avg}$ > 0.12) were observed for residues 14, 42, 43, 59, 75, and 96. The additional cross-peaks of the flexible C-terminus remained unassigned. The 4−108 truncated form of Adx was selected to study protein complex formation in more

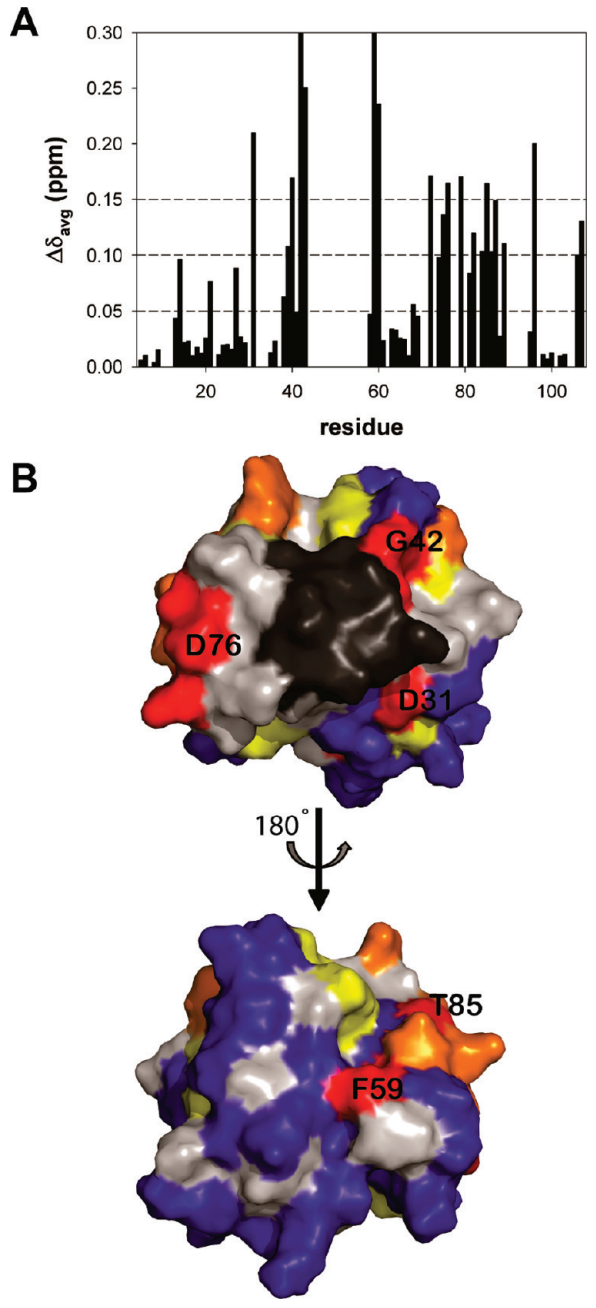

FIGURE 2: Chemical shift perturbation ($\Delta\delta_{avg}$) analysis of $^{2}H^{15}N$ Adx (4−108) after binding of AdR. (A) The obtained $\Delta\delta_{avg}$ of Adx plotted per residue. (B) Chemical shift perturbations mapped on the surface of the protein (structure from PDB entry 1E6E). Residues are color coded according to their $\Delta\delta_{avg}$: larger than 0.15 ppm are colored red, from 0.10 to 0.15 ppm orange, from 0.05 to 0.10 ppm yellow, and less than 0.05 ppm blue. These levels are indicated by dashed lines in (A). The residues for which information was lacking are colored light gray and those broadened beyond detection due to the Fe_2S_2 cluster are colored dark gray.

detail, because Adx (4−108) is more stable than the full-length protein (*45*).

Paramagnetic AdR. To acquire intermolecular distance restraints to steer the docking of AdR and Adx, AdR was equipped with paramagnetic Ln tags. The dipolar interaction between the unpaired electrons of the paramagnetic Ln ions and the observed nuclei of Adx causes broadening and shifts of the NMR resonances in a distance-dependent manner (*46*). CLaNP-5 is a Ln tag that is attached via two Cys residues on the protein surface (Figure 1). It shows minimal mobility relative to the attached protein, and therefore, the paramagnetic effects are large and the Ln ion position is easily modeled (*18*). By attaching Ln-CLaNP-5 at two positions on the AdR surface, one at a time, and adding this tagged AdR to $^{15}N^{2}H$ isotope-enriched Adx, interprotein distance information is obtained from the paramagnetic changes in the NMR spectra of the protein complex. To retrieve pseudocontact shifts, AdR was tagged with CLaNP-5 chelated to Tm^{3+}, for paramagnetic relaxation enhancement Gd-CLaNP-5 was used, and the diamagnetic Lu-CLaNP-5 was taken as a control. In the selection of the AdR variants (see below), Eu-CLaNP-5 was used for its luminescent properties (*18*).

The addition of Ln-CLaNP-5 to wild type AdR led to extensive loss of the FAD cofactor and large amounts of aggregated protein. The cause of this was thought to be binding of the tag to endogenous Cys residues, causing unfolding of the protein. According to the AdR crystal structure, only the thiol of C145 is somewhat surface accessible. Nevertheless, to prevent the aggregation, all five endogenous Cys residues were mutated to Ser, but this AdR variant did not yield correctly folded protein. Then, single Cys to Ser mutants were made and tested for diminished binding of Eu-CLaNP-5, as compared to wild type. The protein stability was monitored by gel filtration chromatography. AdR variant C364S showed highly increased stability toward tag treatment, and only a limited amount of labeling was observed by correlating the Ln-tag fluorescence with flavin-based protein absorbance (data not shown). C364 is in the NADPH binding site. Probably the Ln tag can enter this site and subsequently attach to C364, which leads to loss of the FAD cofactor and aggregation of the protein. Therefore, the C364S mutant was used as the starting point to make double Cys surface mutants, required for CLaNP-5 attachment.

Positions for the Ln tag on AdR were selected 25−35 Å away from the expected binding site of Adx, in rigid parts of the protein. Cys mutations were designed preferably replacing one or two Lys or Arg residues, to reduce the charge change upon attachment of the CLaNP-5, which has a 3+ overall charge. It was decided to make four double Cys mutants indicated with A, B, C, and D (see Materials and Methods section), more than required for obtaining docking restraints. Without optimization, mutants A and B displayed excellent labeling efficiencies, whereas for C and D this was not the case. Although optimization of the labeling procedure would have been possible, it was deemed not practical or necessary, because the study could be completed using only mutants A and B.

AdR Mutant Characterization. AdR mutants A and B were produced and compared to the wild type enzyme. The three proteins displayed the same characteristic UV/vis spectra indicative of a correctly incorporated FAD (*19*) (Figure S3 of the Supporting Information). Furthermore, both AdR mutants also showed the same CD spectra as the wild type, confirming that there are no severe structure differences introduced in the FAD region. The AdR mutants were capable of reducing Adx, as indicated by the changes in the Adx spectra (Figure S3 of the Supporting Information). To quantify Adx reduction by the mutants, the nonphysiological acceptor cytochrome *c* was used (*23*, *29*). Both mutants displayed somewhat higher K_m values and slightly lower V_{max} values than the wild-type enzyme for the reduction of both full-length and truncated Adx, but no severe loss of activity was observed (Table 1).

The AdR mutants were also used to convert 7-dehydrocholesterol (7-DHC) to 7-dehydropregnenolone (7-DHP) in a reconstituted CYP11A1 system. During substrate conversion both

Table 1: Activity of AdR Wild Type and Mutants

	full-length Adx		Adx (4−108)	
AdR	K_m (μM)[a]	V_{max} (nmol of Cyt *c* red/min)[a]	K_m (μM)[a]	V_{max} (nmol of Cyt *c* red/min)[a]
wild type	0.4 ± 0.2	(4.6 ± 0.6) × 10^2	0.6 ± 0.2	(4.8 ± 0.7) × 10^2
mutant A	1.3 ± 0.5	(3.1 ± 0.9) × 10^2	1.7 ± 0.5	(3.8 ± 0.6) × 10^2
mutant B	0.8 ± 0.1	(3.7 ± 0.3) × 10^2	0.8 ± 0.1	(4.3 ± 0.3) × 10^2

[a]The assay conditions are reported in the Materials and Methods section.

Table 2: CYP11A1-Dependent Conversion of 7-Dehydrocholesterol to 7-Dehydropregnenolone

	k_{cat} (s^{-1} × 10^{-3})[a]	
AdR	full-length Adx	Adx (4−108)
wild type	13.4 ± 0.3	22.8 ± 0.1
mutant A	12.4 ± 0.1	20.5 ± 0.7
mutant B	13.3 ± 0.1	22.0 ± 0.3

[a]The assay conditions are reported in the Materials and Methods section.

AdR mutants showed only slight differences compared to wild type AdR for both Adx forms (Table 2). Similar to what was described before, product formation was found to be 60% higher with the truncated Adx as compared to the full-length protein (*47*).

Intermolecular Distance Restraints. AdR mutants A and B were labeled with Lu-CLaNP-5 and Tm-CLaNP-5, to C425/C429 and C232/C236, respectively, and added to $^2H^{15}N$-enriched Adx (4−108). [^1H,^{15}N]-TROSY spectra were acquired for all complexes (Figure S4 of the Supporting Information), and pseudocontact shifts were determined from the chemical shift difference between the paramagnetic and the diamagnetic samples. The two AdR variants labeled with the diamagnetic tag caused the same changes in the TROSY spectrum of Adx (4−108) as did wild type AdR, indicating that labeling with Ln-CLaNP-5 did not affect complex formation between AdR and Adx. The paramagnetic tags caused pseudocontact shifts ranging from 0.1 to less than −1 ppm (Figure 3). No residual diamagnetic peaks were observed in the paramagnetic samples, indicative of complete labeling. Tm-CLaNP-5 is a strong alignment agent, giving rise to HN residual dipolar couplings of up to 30 Hz at 14.1 T (*18*). Consequently, an error is introduced of half the HN residual dipolar coupling in pseudocontact shifts obtained from the TROSY cross-peaks, which may be up to 0.025 ppm for the proton. This value is small relative to the observed pseudocontact shift and was neglected.

To obtain paramagnetic relaxation enhancement based restraints, AdR mutant B was labeled with Gd-CLaNP-5. Paramagnetic relaxation enhancements were determined from the intensity decreases in the TROSY cross-peaks of Adx (Figure S5 of the Supporting Information). The intensity ratios of the paramagnetic and diamagnetic signals are mapped on the crystal structure of Adx in Figure 4. Adx is facing the Ln tag with the small helix consisting of residues 61−64 and the loop containing residue 86.

The Structure of the AdR−Adx Complex. The solution structure of the complex was modeled by docking Adx on AdR, guided by the experimentally obtained chemical shift perturbations, pseudocontact shifts, and paramagnetic relaxation enhancements as intermolecular restraints. The starting structures

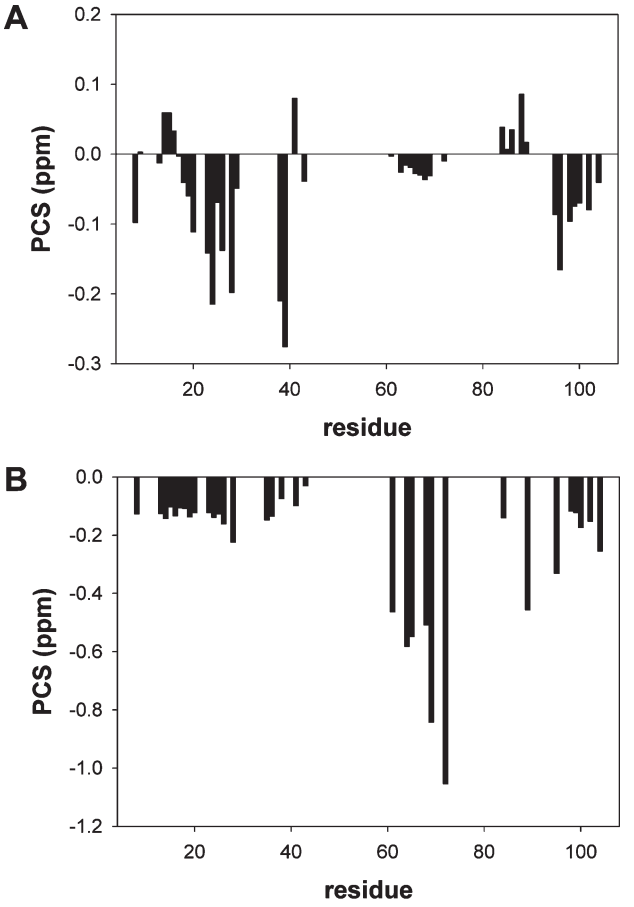

FIGURE 3: Pseudocontact shifts (PCSs) of $^2H^{15}N$ Adx (4−108) in complex with Tm-CLaNP-5 AdR mutants A and B (A and B, respectively) plotted per residue. The pseudocontact shifts were obtained as described in the Materials and Methods section.

of AdR and Adx were taken from the crystallized complex and the free protein, respectively (PDB entries 1E6E and 1AYF), and treated as rigid bodies. AdR was equipped with Ln ions and accompanying initial χ-tensors according to a protocol described before (*18*). During the docking, the orientation of the χ-tensors was optimized in an iterative fashion. The details of the protocol are given in the Materials and Methods section. The lowest energy complex structure is shown in Figure 5A, overlaid with 1E6E, with the AdR molecules superimposed. The location and orientation of Adx on AdR are very similar for the solution model and crystal complex. In both structures the Adx molecules are equally far from the Ln ions. For instance, the distance from the Ln ion in AdR mutant A, attached via C425 and C429, to the Cα of Adx N37 is 30.8 and 31.8 Å in the crystal and the best docking solution, respectively. Similarly, the distance from the other Ln ion, attached via C232 and C236, in AdR mutant B, is 23.3 and 23.6 Å to the Cα of D86 of the crystal structure and the best docking solution, respectively.

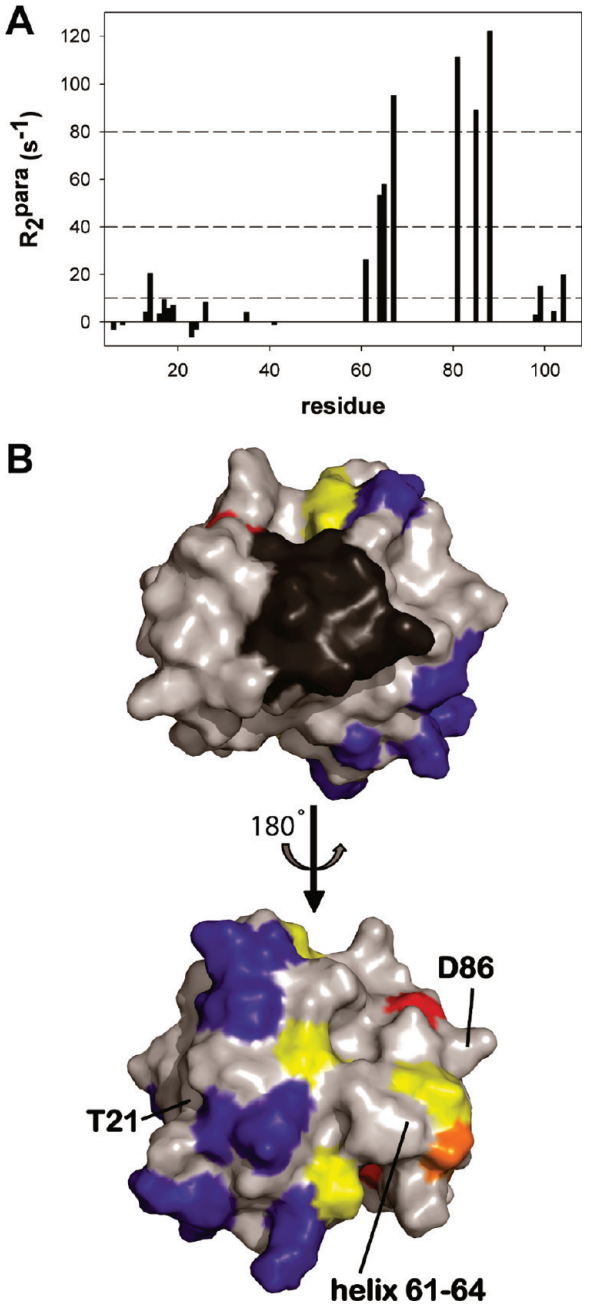

FIGURE 4: Analysis of paramagnetic relaxation enhancement of the $^2H^{15}N$ Adx (4−108) resonances by bound AdR mutant B with Gd-CLaNP-5 attached. (A) The observed R_2^{para} plotted per residue. (B) The observed R_2^{para} mapped on the surface of the protein, with $R_2^{para} > 80\ s^{-1}$ in red, $40 < R_2^{para} < 80\ s^{-1}$ in orange, $10 < R_2^{para} < 40\ s^{-1}$ in yellow, and $R_2^{para} < 10\ s^{-1}$ in blue. These levels are indicated by dashed lines in (A). The residues for which information was lacking are colored light gray, and those broadened beyond detection due to the Fe_2S_2 cluster are colored dark gray.

Relative to the crystal structure, in the lowest energy solution Adx is slightly rotated around the core β-sheets consisting of residues 56−58 and 88−90. The Cα atoms of H56 are only 0.7 Å apart and the Cα atoms of L90 1.8 Å. The loop of Adx containing the Fe_2S_2 cluster is tilted to a small extent in the lowest energy solution. This tilt causes the distance between the closest iron atom of the Fe_2S_2 cluster and the FAD isoalloxazine ring N3 atom to increase from 10.9 to 15.0 Å. This is still within the critical electron transfer distance of 16 Å (*48*).

The total energy of the best docking solution is 19% lower than that of the crystal structure after χ-tensor optimization, 13.3 kcal/mol compared to 15.8 kcal/mol. This is reflected in the *Q*-value, that measures the agreement between back-predicted and experimental pseudocontact shifts and paramagnetic relaxation enhancement based distances (Figure 5B−D). *Q*, averaged over the pseudocontact shifts and paramagnetic relaxation enhancement classes of restraints, equals 0.110 and 0.102 for the crystal structure and solution model, respectively. The lower *Q*-value of the solution model can be attributed to a large extent to the Ln tag attached to residues 425 and 429 (AdR mutant B). The *Q*-values for the pseudocontact shifts originating from this tag are 0.23 and 0.21 for the crystal structure and solution model, respectively.

The rmsd between the lowest energy solution from the docking and the crystal structure is 6.4 Å, with a distance root mean square (drms) of 2.5 Å. The difference between the rmsd and the drms is a consequence of the fact that the structures are rotated rather than translated (*49*).

Single Minimum. For the ensemble of low-energy structures obtained during the docking calculations the restraint energy is plotted against the rmsd relative to the lowest energy structure in Figure 6A. As shown in the figure, the docking appears to converge to a single minimum. All low-energy structures were similar, with Adx bound in the groove between the FAD domain and the NADPH domain of AdR and the Adx Fe_2S_2 cluster facing the FAD isoalloxazine ring. The centers of mass of Adx of the top ten of low-energy solutions are displayed in Figure 6B. These structures can all be found on a straight line equidistant from the Ln ions, in the groove between the two AdR domains. The farther the structure is from the minimum, the higher the total energy. The crystal structure is found within the cloud. The top ten low-energy structures form a cloud with an rmsd from the mean of 3.2 Å.

As can be seen in Figure 6C,D, during the optimization the χ-tensors rotate mostly in the *xy*-plane whereas the *z*-axis is similar in all low-energy solutions; only inversion is observed. The fact that the *x*- and *y*-axes display some freedom of movement can be explained by the relatively low rhombicity of the χ-tensor, making the pseudocontact shifts less sensitive to changes in the *x*- and *y*-axes. The largest deviations of the average χ-tensors are found for the structures with the highest total energies.

The outcome of the docking procedure is of course sensitive to the relative weights given to the different restraints. The weights for the paramagnetic relaxation enhancements and pseudocontact shifts were chosen such that the energy terms for both were of similar magnitude and that both energy terms contribute to the ranking of the lowest energy structures. This was based on the assumption that both classes of restraints are equally important. A possible source of error for the calculation of atomic distances from paramagnetic relaxation enhancements is τ_c. Based upon the crystallized complex, τ_c was estimated by HYDRONMR (*50*) to be 52.0 ns. The influence of τ_c was verified by varying it from 43.0 to 57.0 ns and comparing the paramagnetic relaxation enhancement based amide to Ln distances with the distances from the best docking structure. The lowest *Q*-factor (considering only paramagnetic relaxation enhancement derived distances) was obtained for a value of 47.0 ns (Figure S6 of the Supporting Information). However, the influence of τ_c remains within the error in the *Q*-factor at least in the range from 43 to 53 ns, and simulations performed with τ_c set to 47 or 49 ns gave similar results.

Dependence of the Docking on the Adx Starting Conformation. This study aims to provide a methodology for

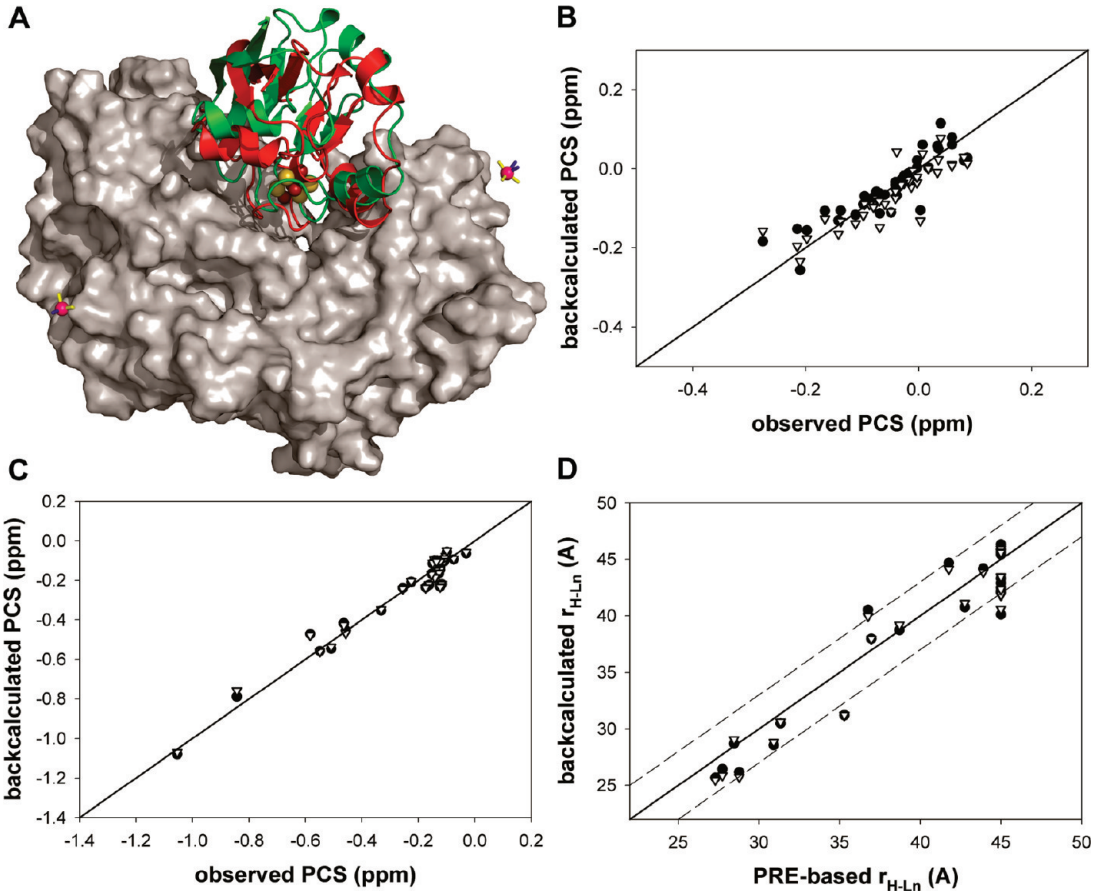

FIGURE 5: Structural comparison of the docking solution and the crystal structure. (A) The lowest energy docking solution of the AdR−Adx complex superimposed on the crystal structure of the complex (PDB entry 1E6E). The structures are aligned by AdR, which is shown in surface representation. The Ln ion positions are indicated by pink spheres, with the axis frame representing the χ-tensor of Tm in yellow for the *x*- and *y*-axes and in blue for the *z*-axes. The positions of Adx as determined by NMR and in the crystal structure are shown as green and red cartoons, respectively. The Fe_2S_2 clusters are shown as spheres in CPK colors. (B, C) Plots of the pseudocontact shifts (PCSs) back-calculated from the lowest energy docking solution (●) and the crystal structure (▽) against the experimental data are shown in (B) and (C) for AdR mutants A and B, respectively. (D) The Gd-to-H^N distances back-calculated from the lowest energy docking solution (●) and the crystal structure (▽) are plotted against the experimental paramagnetic relaxation enhancement (PRE) based distances. The solid lines represent the ideal correlation, and dashed lines in (D) represent the 3 Å error margins used in the analysis. *Q*-values are for (B) 0.210 (●) and 0.233 (▽), for (C) 0.065 (●) and 0.067 (▽), and for (D) 0.031 (●) and 0.030 (▽).

finding a structure of a protein complex based on any given structures of the free components, so the effect of different starting structures should be small. The docking calculations were repeated with different Adx structures, taken from crystal structures of Adx in complex with AdR (PDB entry 1E6E) and as a free oxidized protein (PDB entry 1CJE). For any of the three Adx structures, a single minimum was found in the docking calculations. The lowest energy solutions are very similar to the one obtained using 1AYF-based Adx (Figure S7 of the Supporting Information). The backbone rmsd of Adx in the three complexes, aligned by AdR, is only 0.9 Å, so it can be concluded that the same minimum energy structure of the complex is found independent of the starting structure, in accord with the similarity between the three Adx structures (backbone rmsd to the mean is 0.3 Å).

The top ten lowest energy solutions, using the Adx structure from 1CJE and 1E6E, form an ensemble with a backbone rmsd of 2.5 and 2.1 Å, respectively. Apparently, the accuracy of the calculations is determined by the experimental restraints, whereas the precision is dependent on the starting structures. The best solution of the calculation starting with Adx from the crystallized complex (1E6E) also has a somewhat lower energy compared to the other two, 12.0 versus 13.3 and 13.7 kcal/mol for 1AYF and 1CJE, respectively, and consequently, also the *Q*-value for the fits of back-calculated to the experimental restraints is a little lower, 0.098 versus 0.102 and 0.102. These findings show that side-chain orientations have little influence on the orientation determined for Adx in the complex but result in a slightly better fit if already optimized for binding. This limited influence is a consequence of the "soft docking" used in the protocol, with only the backbone atoms and Cβ and Cγ taken into account for the repel term in the docking energy.

Methods for Protein Complex Structure Determination. The combination of chemical shift perturbation, pseudocontact shift, and paramagnetic relaxation enhancement restraints was successfully used to obtain a model of the complex formed by AdR and Adx in solution. We have also investigated whether all restraints were required to obtain a reliable solution.

Several software packages such as Bigger and Haddock (*51*, *52*) are available for the prediction of structures of protein complexes based on a minimal set of experimental restraints, often giving excellent results. Haddock was employed (*53*), to dock Adx on AdR, using the experimental chemical shift perturbations as restraints. In the best docking solution, Adx was placed in between the FAD and NADPH domains of AdR, but on the opposite side of the isoalloxazine ring (Figure S8 of the Supporting

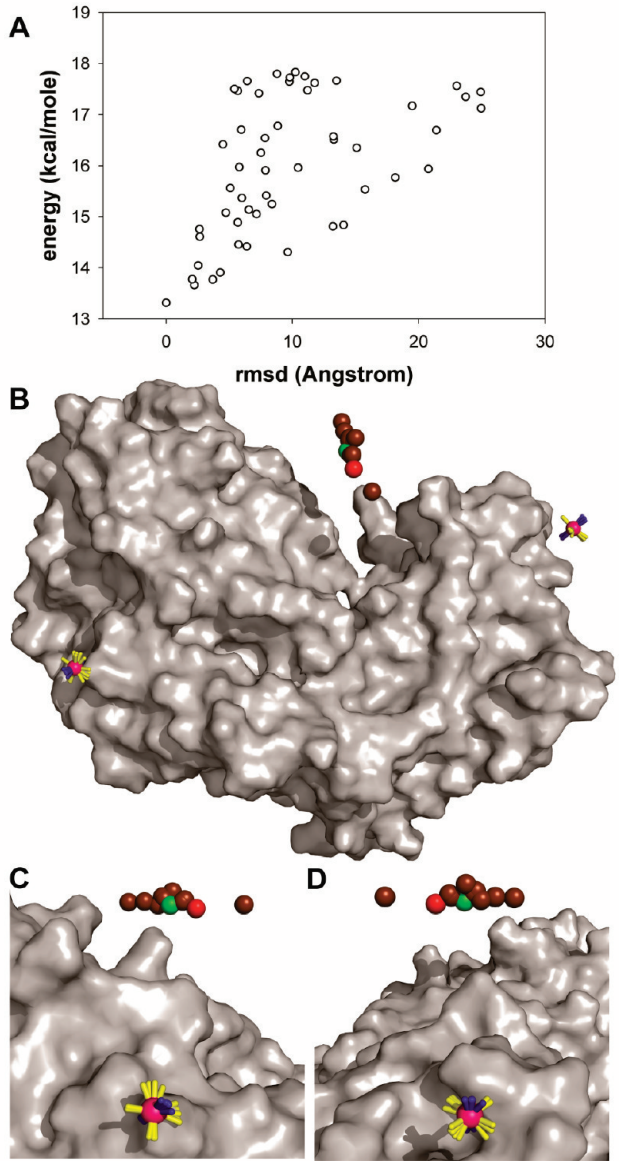

FIGURE 6: Population analysis of the low-energy solutions from the docking of Adx on AdR. (A) The energies of the docking solutions are plotted against their rmsd relative to the lowest energy structure. (B) The top ten lowest energy docking solutions of the Adx−AdR complex are shown. AdR is displayed in surface representation. Centers of mass of Adx are displayed as spheres, with the lowest energy solution in green, the crystal structure in red, and the others in brown. The Ln ion positions are indicated by pink spheres, with the axis frame representing the χ-tensor of Tm in yellow for the x- and y-axes and in blue for the z-axes. (C, D) Detailed views of the χ-tensors of the Tm ions attached to mutants A and B, respectively.

Information). In the second best solution Adx was placed at the same place as in the crystallized complex, but rotated. Similar results were obtained when the docking was performed in XPLOR, using only the chemical shift perturbation restraints (Figure S9 of the Supporting Information). Many of the solutions were found with Adx in the groove between the NADPH domain and the FAD domain. Like with Haddock, in the lowest energy structure the Fe_2S_2 cluster of Adx was facing the back of the FAD in AdR. Therefore, to determine the solution structure of the AdR−Adx complex, additional information about the binding site on AdR is required.

Including the chemical shift perturbation and pseudocontact shift but not the paramagnetic relaxation enhancement restraints

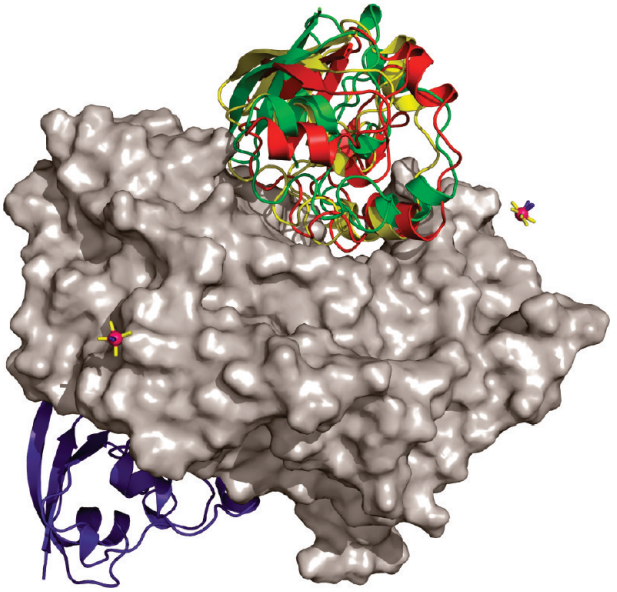

FIGURE 7: The structures of the lowest energy solutions of the Adx−AdR complex using increasingly more experimental restraints. Adx structures are shown as cartoons, in blue using chemical shift perturbations only, in yellow using chemical shift perturbations and pseudocontact shifts, and in green using chemical shift perturbations, pseudocontact shifts, and paramagnetic relaxation enhancements, and Adx from the crystal complex is in red. AdR is displayed as a gray surface-filled structure and the Ln ion positions are indicated by pink spheres, with an axis frame representing the χ-tensor of Tm in yellow for the x- and y-axes and in blue for the z-axes.

yielded a clear minimum as well with Adx facing the FAD isoalloxazine ring with its Fe_2S_2 cluster. There are only small differences with the model obtained when the paramagnetic relaxation enhancements are included. In the best structure obtained without the paramagnetic relaxation enhancement restraints, the Fe_2S_2 cluster is rotated only 0.5 Å further away from the FAD. The ten lowest energy structures form a cloud of similar structures with an rmsd of 2.4 Å from the mean (Figure S10 of the Supporting Information). The crystal structure has a backbone rmsd of 3.1 Å with the mean of this ensemble. So with only chemical shift perturbation and pseudocontact shift restraints originating from two Ln positions it is possible to retrieve a model of the complex with reasonable resolution. Apparently, the addition of the paramagnetic relaxation enhancement restraints to the docking does not significantly change the outcome of the docking. The lowest energy models obtained using increasing sets of restraints are shown in Figure 7.

In principle, residual dipolar couplings could also aid in structure determination. Ln-CLaNP-5 is a strong alignment agent (*54*, *55*), potentially yielding the residual dipolar couplings that can be used to refine protein structure (*56*). Unfortunately, to deconvolute the residual dipolar coupling and pseudocontact shift contributions to the paramagnetic shift in the TROSY spectra, the antiTROSY spectrum is required as well. For the low-concentration samples of the AdR−Adx complex, the sensitivity required for the anti-TROSY spectra could not be achieved.

Solution versus Crystal Structure. The fact that the best docking solution is highly similar to the crystallized complex answers the longstanding question about the physiological relevance of the cross-linked crystal structure. In this study, we show that the crystallized complex structure fulfills the experimental restraints found in solution by NMR very well (Figure 5). In the crystal structure, Adx D39 and AdR K27 are chemically

cross-linked. Although this artificial covalent binding may have had an effect on the crystallized complex, the distances between Adx and AdR in the solution model are not very different from those in the crystallized complex. For instance, the distance between D39 and K27 decreases from 8.9 to 7.6 Å (Cα to Cα); therefore, a cross-link between these residues as in the crystal does not seem to be physically impossible.

CONCLUSIONS

We have established a model for the 65 kDa protein complex formed in solution by AdR and Adx and found that this structure is very similar to the crystallized complex of chemically cross-linked AdR and Adx. The solution model was obtained using TROSY NMR experiments in combination with perdeuteration of the observed protein on the basis of paramagnetic restraints, delivered by two Ln tags. Because of the strength and rigidity of the Ln tag, significant long-range distance restraints up to 56 Å could be obtained, even though the amount of AdR was limited. Furthermore, the presence of the iron−sulfur cluster in Adx makes the interface residues invisible in NMR experiments, so only nuclei of Adx far from the interface could be studied. Therefore, the paramagnetic NMR approach, using rigid Ln tags, seems well suited as a general tool to determine structures of difficult, large and poorly available targets.

ACKNOWLEDGMENT

We thank Dr. Hans Wienk and the NMR facility of the Bijvoet Center in Utrecht for technical assistance and use of the spectrometers.

SUPPORTING INFORMATION AVAILABLE

NMR spectra, wild-type Adx binding map, mutant AdR validation, τ_c optimization, structures of the AdR−Adx complex, and the XPLOR-NIH docking script. This material is available free of charge via the Internet at http://pubs.acs.org.

REFERENCES

1. Fernández, C., and Wüthrich, K. (2003) NMR solution structure determination of membrane proteins reconstituted in detergent micelles. *FEBS Lett. 555*, 144–150.
2. Grzesiek, S., and Sass, H. J. (2009) From biomolecular structure to functional understanding: new NMR developments narrow the gap. *Curr. Opin. Struct. Biol. 19*, 585–595.
3. Kay, L. E. (2005) NMR studies of protein structure and dynamics. *J. Magn. Reson. 173*, 193–207.
4. Hiller, S., and Wagner, G. (2009) The role of solution NMR in the structure determinations of VDAC-1 and other membrane proteins. *Curr. Opin. Struct. Biol. 19*, 396–401.
5. Bertini, I., Luchinat, C., Parigi, G., and Pierattelli, R. (2005) NMR spectroscopy of paramagnetic metalloproteins. *ChemBioChem 6*, 1536–1549.
6. Xu, X., Reinle, W., Hannemann, F., Konarev, P. V., Svergun, D. I., Bernhardt, R., and Ubbink, M. (2008) Dynamics in a pure encounter complex of two proteins studied by solution scattering and paramagnetic NMR spectroscopy. *J. Am. Chem. Soc. 130*, 6395–6403.
7. Clore, G. M., Tang, C., and Iwahara, J. (2007) Elucidating transient macromolecular interactions using paramagnetic relaxation enhancement. *Curr. Opin. Struct. Biol. 17*, 603–616.
8. Lambeth, J. D. (1990) Enzymology of mitochondrial side-chain cleavage by cytochrome P-450scc, Vol. 3, Akademie-Verlag, Berlin.
9. Bernhardt, R. (1996) Cytochrome P450: structure, function, and generation of reactive oxygen species. *Rev. Physiol., Biochem., Pharmacol. 127*, 137–221.
10. Bernhardt, R. (2006) Cytochromes P450 as versatile biocatalysts. *J. Biotechnol. 124*, 128–145.
11. Ishimura, K., and Fujita, H. (1997) Light and electron microscopic immunohistochemistry of the localization of adrenal steroidogenic enzymes. *Microsc. Res. Tech. 36*, 445–453.
12. Hanukoglu, I. J. (1992) *Steroid Biochem. Mol. Biol. 43*, 779–804.
13. Ziegler, G. A., Vonrhein, C., Hanukoglu, I., and Schulz, G. E. (1999) The structure of adrenodoxin reductase of mitochondrial P450 systems: electron transfer for steroid biosynthesis. *J. Mol. Biol. 289*, 981–990.
14. Muller, A., Muller, J. J., Muller, Y. A., Uhlmann, H., Bernhardt, R., and Heinemann, U. (1998) New aspects of electron transfer revealed by the crystal structure of a truncated bovine adrenodoxin, Adx-(4−108). *Structure 6*, 269–280.
15. Pikuleva, I. A., Tesh, K., Waterman, M. R., and Kim, Y. (2000) The tertiary structure of full-length bovine adrenodoxin suggests functional dimers. *Arch. Biochem. Biophys. 373*, 44–55.
16. Ziegler, G. A., and Schulz, G. E. (2000) Crystal structures of adrenodoxin reductase in complex with $NADP^+$ and NADPH suggesting a mechanism for the electron transfer of an enzyme family. *Biochemistry 39*, 10986–10995.
17. Muller, J. J., Lapko, A., Bourenkov, G., Ruckpaul, K., and Heinemann, U. (2001) Adrenodoxin reductase-adrenodoxin complex structure suggests electron transfer path in steroid biosynthesis. *J. Biol. Chem. 276*, 2786–2789.
18. Keizers, P. H. J., Saragliadis, A., Hiruma, Y., Overhand, M., and Ubbink, M. (2008) Design, synthesis, and evaluation of a lanthanide chelating protein probe: CLaNP-5 yields predictable paramagnetic effects independent of environment. *J. Am. Chem. Soc. 130*, 14802–14812.
19. Sagara, Y., Wada, A., Takata, Y., Waterman, M. R., Sekimizu, K., and Horiuchi, T. (1993) Direct expression of adrenodoxin reductase in *Escherichia coli* and the functional characterization. *Biol. Pharm. Bull. 16*, 627–630.
20. Miroux, B., and Walker, J. E. (1996) Over-production of proteins in *Escherichia coli*: mutant hosts that allow synthesis of some membrane proteins and globular proteins at high levels. *J. Mol. Biol. 260*, 289–298.
21. Nishihara, K., Kanemori, M., Kitagawa, M., Yanagi, H., and Yura, T. (1998) Chaperone coexpression plasmids: differential and synergistic roles of DnaK-DnaJ-GrpE and GroEL-GroES in assisting folding of an allergen of Japanese cedar pollen, Cryj2, in *Escherichia coli*. *Appl. Environ. Microbiol. 64*, 1694–1699.
22. Hiwatashi, A., Ichikawa, Y., Maruya, N., Yamano, T., and Aki, K. (1976) Properties of crystalline reduced nicotinamide adenine dinucleotide phosphate-adrenodoxin reductase from bovine adrenocortical mitochonria. I. Physicochemical properties of holo- and apo-NADPH-adrenodoxin reductase and interaction between non-heme iron proteins and the reductase. *Biochemistry 15*, 3082–3090.
23. Uhlmann, H., Kraft, R., and Bernhardt, R. (1994) C-terminal region of adrenodoxin affects its structural integrity and determines differences in its electron transfer function to cytochrome P-450. *J. Biol. Chem. 269*, 22557–22564.
24. Worrall, J. A., Reinle, W., Bernhardt, R., and Ubbink, M. (2003) Transient protein interactions studied by NMR spectroscopy: the case of cytochrome C and adrenodoxin. *Biochemistry 42*, 7068–7076.
25. Schiffler, B., Zollner, A., and Bernhardt, R. (2004) Stripping down the mitochondrial cholesterol hydroxylase system, a kinetics study. *J. Biol. Chem. 279*, 34269–34276.
26. Huang, J. J., and Kimura, T. (1973) Studies on adrenal steroid hydroxylases. Oxidation-reduction properties of adrenal iron-sulfur protein (adrenodoxin). *Biochemistry 12*, 406–409.
27. Pikuleva, I. A., Mackman, R. L., Kagawa, N., Waterman, M. R., and Ortiz de Montellano, P. R. (1995) Active-site topology of bovine cholesterol side-chain cleavage cytochrome P450 (P450scc) and evidence for interaction of tyrosine 94 with the side chain of cholesterol. *Arch. Biochem. Biophys. 322*, 189–197.
28. Omura, T., and Sato, R. (1964) The carbon monoxide-binding pigment of liver microsomes. II. Solubilization, purification and properties. *J. Biol. Chem. 239*, 2379–2385.
29. Lambeth, J. D., Seybert, D. W., and Kamin, H. (1979) Ionic effects on adrenal steroidogenic electron transport. The role of adrenodoxin as an electron shuttle. *J. Biol. Chem. 254*, 7255–7264.
30. Massey, V. (1959) The microestimation of succinate and the extinction coefficient of cytochrome *c*. *Biochim. Biophys. Acta 34*, 255–256.
31. Sugano, S., Miura, R., and Morishima, N. (1996) Identification of intermediates in the conversion of cholesterol to pregnenolone with a reconstituted cytochrome p-450scc system: accumulation of the intermediate modulated by the adrenodoxin level. *J. Biochem. 120*, 780–787.
32. Pervushin, K., Riek, R., Wider, G., and Wüthrich, K. (1997) Attenuated T2 relaxation by mutual cancellation of dipole-dipole coupling and chemical shift anisotropy indicates an avenue to NMR structures of very large biological macromolecules in solution. *Proc. Natl. Acad. Sci. U.S.A. 94*, 12366–12371.

33. Helgstrand, M., Kraulis, P., Allard, P., and Hard, T. (2000) Ansig for Windows: an interactive computer program for semiautomatic assignment of protein NMR spectra. *J. Biomol. NMR 18*, 329–336.
34. Xu, X., Kim, S. K., Schurmann, P., Hirasawa, M., Tripathy, J. N., Smith, J., Knaff, D. B., and Ubbink, M. (2006) Ferredoxin/ferredoxin-thioredoxin reductase complex: complete NMR mapping of the interaction site on ferredoxin by gallium substitution. *FEBS Lett. 580*, 6714–6720.
35. Grzesiek, S., Bax, A., Clore, G. M., Gronenborn, A. M., Hu, J., Kaufman, J., Palmer, I., Stahl, S. J., and Wingfield, P. T. (1996) The solution structure of HIV-1 Nef reveals an unexpected fold and permits delineation of the binding surface for the SH3 domain of Hck tyrosine protein kinase. *Nat. Struct. Biol. 3*, 340–345.
36. Bashir, Q., Volkov, A. N., Ullmann, G. M., and Ubbink, M. (2010) Visualization of the encounter ensemble of the transient electron transfer complex of cytochrome *c* and cytochrome *c* peroxidase. *J. Am. Chem. Soc. 132*, 241–247.
37. Solomon, I., and Bloembergen, N. (1956) Nuclear magnetic interactions in the HF molecule. *J. Chem. Phys. 25*, 261–266.
38. Battiste, J. L., and Wagner, G. (2000) Utilization of site-directed spin labeling and high-resolution heteronuclear nuclear magnetic resonance for global fold determination of large proteins with limited nuclear overhauser effect data. *Biochemistry 39*, 5355–5365.
39. Iwahara, J., Tang, C., and Clore, G. M. (2007) Practical aspects of (1)H transverse paramagnetic relaxation enhancement measurements on macromolecules. *J. Magn. Reson. 184*, 185–195.
40. Vlasie, M. D., Fernandez-Busnadiego, R., Prudencio, M., and Ubbink, M. (2008) Conformation of pseudoazurin in the 152 kDa electron transfer complex with nitrite reductase determined by paramagnetic NMR. *J. Mol. Biol. 375*, 1405–1415.
41. Schwieters, C. D., Kuszewski, J. J., Tjandra, N., and Clore, G. M. (2003) The Xplor-NIH NMR molecular structure determination package. *J. Magn. Reson. 160*, 65–73.
42. Banci, L., Bertini, I., Cavallaro, G., Giachetti, A., Luchinat, C., and Parigi, G. (2004) Paramagnetism-based restraints for Xplor-NIH. *J. Biomol. NMR 28*, 249–261.
43. van Aalten, D. M., Bywater, R., Findlay, J. B., Hendlich, M., Hooft, R. W., and Vriend, G. (1996) PRODRG, a program for generating molecular topologies and unique molecular descriptors from coordinates of small molecules. *J. Comput.-Aided Mol. Des. 10*, 255–262.
44. Gerstein, M. (1992) A resolution-sensitive procedure for comparing protein surfaces and its application to the comparison of antigen-combining sites. *Acta Crystallogr., Sect. A 48*, 271–276.
45. Burova, T. V., Beckert, V., Uhlmann, H., Ristau, O., Bernhardt, R., and Pfeil, W. (1996) Conformational stability of adrenodoxin mutant proteins. *Protein Sci. 5*, 1890–1897.
46. Otting, G. (2008) Prospects for lanthanides in structural biology by NMR. *J. Biomol. NMR 42*, 1–9.
47. Schiffler, B., Kiefer, M., Wilken, A., Hannemann, F., Adolph, H. W., and Bernhardt, R. (2001) The interaction of bovine adrenodoxin with CYP11A1 (cytochrome P450scc) and CYP11B1 (cytochrome P45011beta). Acceleration of reduction and substrate conversion by site-directed mutagenesis of adrenodoxin. *J. Biol. Chem. 276*, 36225–36232.
48. Page, C. C., Moser, C. C., Chen, X., and Dutton, P. L. (1999) Natural engineering principles of electron tunnelling in biological oxidation-reduction. *Nature 402*, 47–52.
49. Kim, Y. C., Tang, C., Clore, G. M., and Hummer, G. (2008) Replica exchange simulations of transient encounter complexes in protein-protein association. *Proc. Natl. Acad. Sci. U.S.A. 105*, 12855–12860.
50. Garcia de la Torre, J., Huertas, M. L., and Carrasco, B. (2000) HYDRONMR: prediction of NMR relaxation of globular proteins from atomic-level structures and hydrodynamic calculations. *J. Magn. Reson. 147*, 138–146.
51. Palma, P. N., Krippahl, L., Wampler, J. E., and Moura, J. J. G. (2000) BiGGER: a new (soft) docking algorithm for predicting protein interactions. *Proteins 39*, 372–384.
52. Dominguez, C., Boelens, R., and Bonvin, A. M. (2003) HADDOCK: a protein-protein docking approach based on biochemical or biophysical information. *J. Am. Chem. Soc. 125*, 1731–1737.
53. de Vries, S. J., van Dijk, M., and Bonvin, A. M. (2010) The HADDOCK web server for data-driven biomolecular docking, *Nat. Protoc.* (in press).
54. Keizers, P. H. J., Desreux, J. F., Overhand, M., and Ubbink, M. (2007) Increased paramagnetic effect of a lanthanide protein probe by two-point attachment. *J. Am. Chem. Soc. 129*, 9292–9293.
55. Xu, X., Keizers, P. H., Reinle, W., Hannemann, F., Bernhardt, R., and Ubbink, M. (2009) Intermolecular dynamics studied by paramagnetic tagging. *J. Biomol. NMR 43*, 247–254.
56. Prestegard, J. H., and Kishore, K. I. (2001) Partial alignment of biomolecules: an aid to NMR characterization. *Curr. Opin. Chem. Biol. 5*, 584–590.